Proceedings of the ASME 2017 International Mechanical Engineering Congress and Exposition
IMECE2017
November 3-9, 2017, Tampa, Florida, USA

IMECE2017-71344

CLOSED-LOOP SIGNAL SHAPING WITH INNER-LOOP MODEL MATCHING

Withit Chatlatanagulchai
Department of Mechanical Engineering
Faculty of Engineering
Kasetsart University
Chatuchak, Bangkok, Thailand

Kittipong Yaovaja
Department of Mechanical Engineering
Faculty of Engineering at Sriracha
Kasetsart University Sriracha Campus
Sriracha, Chonburi, Thailand

Puwadon Poedaeng
Department of Mechanical Engineering
Faculty of Engineering
Kasetsart University
Chatuchak, Bangkok, Thailand

ABSTRACT

Input shaper is a pre-filter, designed to suppress residual vibration of flexible systems. The input shaper can be placed inside the feedback loop, in front of the flexible plant, to avoid exciting the plant vibratory modes. The performance of this so-called closed-loop signal shaping is limited due to the time delay brought about by the input shaper. The input shaper has more time delay when the plant mode parameters are uncertain. In this paper, an inner-loop controller based on the quantitative feedback theory is designed to match the uncertain flexible plant to a reference model. As a result, the input shaper needs not be robust, and the time delay is reduced. Other benefits include shorter input shaper length, increasing controller bandwidth, applicable to time-varying plant, and reducing cost of feedback. Simulation and experiment have confirmed the effectiveness of the newly proposed technique.

INTRODUCTION

Residual vibration takes place when moving a flexible system rapidly from point to point. Input shaping is a simple technique used to suppress this vibration by shaping the signal so that it will not excite the vibratory modes of the flexible plant. Input shaping is based on the idea presented in [1].

Recently, the input shaper is placed inside the feedback loop, so-called *closed-loop signal shaping (CLSS)* [2], to gain benefits such as eliminating the vibration induced by plant-output disturbance, ease in stabilizing the non-collocated systems, ease in handling hard nonlinearities (backlash, deadzone, saturation), and improving performance of manual control. Recently, the CLSS has been applied to actual systems including bridge crane with distributed mass [3], 3D crane with PID controller [4], and helicopter [5].

Disadvantages of CLSS, pointed out in [6], include the inability to suppress the vibration induced by the plant-input disturbance, the unexpected instability from inaccurate plant model, and, most importantly, the detrimental effect from introducing time delays in the feedback loop.

The input shaper contains time delays. These time delays are larger when the time duration or length of the input shaper increases. Longer input shaper is required when the plant model is inaccurate.

Reference model matching has recently been proposed to match the uncertain plant model to an exact reference model. The input shaper can then be designed using the exact reference model. Several model matching techniques, proposed with the input shaper, include neuro-sliding mode controller [7], acceleration feedback [8], state-feedback with two gains [9], output decomposition [10], proportional-integral controller [11], Lyapunov-based controller [12], iterative learning controller [13], and quantitative feedback controller [14].

In this paper, the quantitative feedback controller [15] is used as the inner-loop feedback controller to match the uncertain flexible plant to an exact reference model. The input shaper is placed before the inner-loop system and is designed from the exact reference model. A proportional-integral controller is used in the outer-loop system for reference signal tracking.

The advantages of the proposed technique over traditional CLSS are as follows:

- Shorter input shaper length is required. Because the input shaper is designed from an exact reference model, it does not need to be robust; therefore, the length can be shorten.

- Controller bandwidth is increased due to less time delay from shorter input shaper length.

- The technique can be applied to time-varying or nonlinear plants because the inner-loop controller matches the varying plant to an exact reference model.

PROPOSED SYSTEM

The proposed system is shown in Fig. 1. *P* is the flexible plant. *F*, *G*, and *C* are the controllers to be designed. *IS* is the input shaper. *y* is the flexible-body output. *u* is the control effort from *G*. *e* is the error signal of the inner loop. r_s is the shaped reference for the inner loop. *v* is the control effort from *C*. r_b is the baseline reference. F_m is the reference model for the inner loop.

P can be uncertain, leading to lengthy *IS*. As a remedy, *F* and *G* are the inner-loop controllers, designed to match the inner-loop system to an exact reference model, F_m. As a result, *IS* can have a shorter duration because it does not need to be robust. A shorter-duration *IS* means less time delay in the loop, which increases control bandwidth for *C*.

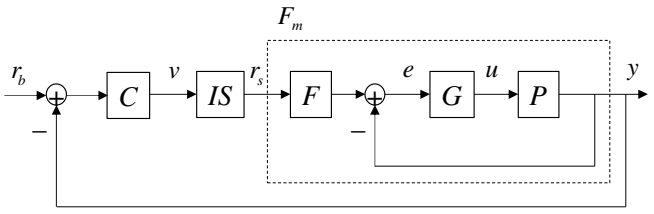

Fig. 1 Closed-loop signal shaping with inner-loop model matching.

In this paper, a proportional-integral (PI) controller was used as *C*. *F* and *G* were designed using the quantitative feedback theory (QFT) to cover all possible uncertain plant, *P*.

F_m is an underdamped system that is handled by *IS*. Letting F_m be underdamped, instead of overdamped or critically damped, reduces the cost of feedback because *IS* is a feed-forward filter.

A. Plant, P

A two-mass rigid-flexible plant, as shown in Fig. 2, represents many flexible plants in practice. It also represents the flexible-joint robot, which was used as experimental hardware in this paper.

The objective is to command the flexible output, $y = x_2$, to follow the baseline reference, r_b, without residual vibration at the end point.

The transfer function from the control effort, *u*, to the flexible output, $y = x_2$, is given by

$$P(s) = \frac{Y}{U} = \frac{c_2 s + k_2}{\left[\begin{array}{l}(m_1 m_2)s^4 + (m_1 c_2 + c_1 m_2 + c_2 m_2)s^3 \\ +(m_1 k_2 + c_1 c_2 + k_2 m_2)s^2 + (c_1 k_2)s\end{array}\right]},$$

where c_1 and c_2 are the damping constants, k_2 is the spring stiffness, m_1 and m_2 are the rigid and the flexible masses.

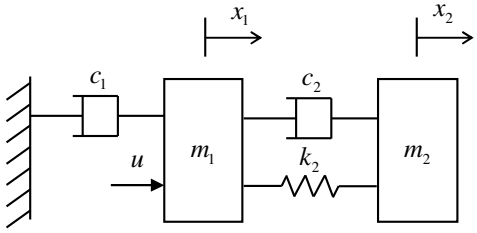

Fig. 2 Two-mass rigid-flexible plant.

In simulation, the following parameter values were used: $m_1 = 10$ kg, $m_2 = 1$ kg, $c_1 = 50$ kg/s, $c_2 = 0.1$ kg/s, and $k_2 = 10$ kg/s^2.

The natural frequency and damping ratio of the plant were computed as $\omega_n = 3.2074$ rad/s and $\zeta = 0.0389$. Therefore, a natural choice for the reference model, F_m, is a second-order model:

$$F_m(s) = \frac{(3.2074)^2}{s^2 + 2(0.0389)(3.2074)s + (3.2074)^2}. \quad (1)$$

B. Inner-Loop Controllers, F and G

In simulation, c_1, c_2, and k_2 were allowed to have 50% uncertainty, that is, $c_1 \in \{25, 50, 75\}$, $c_2 \in \{0.05, 0.1, 0.15\}$, and $k_2 \in \{5, 10, 15\}$. Therefore, there are $3^3 = 27$ possible plants, *P*, with the 14th case as the nominal plant.

For all 27 possible plants, the controller, *G*, and the prefilter, *F*, were designed to meet the stability margin specification

$$\left|\frac{PG}{1+PG}\right| < 3 \text{ dB} = 1.413 \quad (2)$$

and the model matching specification

$$\left|\frac{PGF}{1+PG} - F_m\right| < -20 \text{ dB} = 0.1, \quad (3)$$

using a loop shaping technique called *quantitative feedback theory* [15].

Fig. 3 shows the worst-case bounds, obtained from the stability margin and the model matching specifications, on the Nichols chart. There are 8 frequencies of interest, from 0.05 rad/s to 20 rad/s, covering low, high, and natural frequency of the plant. Fig. 3 also contains the original open-loop shape of $L = PG$, where $G = 1$.

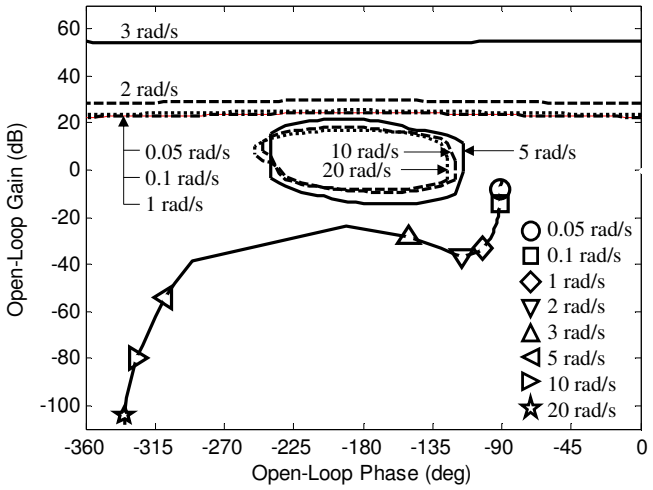

Fig. 3 Open-loop shaping: original shape.

To satisfy all the bounds, the open-loop shape must be altered so that each frequency point lies in the allowable region, which in this case is above or outside the bound. Therefore, the original open-loop shape must be moved upward and to the right of the Nichols chart.

To do so, the open-loop gain was increased. A real zero and a complex zero were appended to help increase the open-loop gain and phase. The final controller, G, after the loop shaping is given by

$$G = 87.367\left(s + 17.24\right)\left(s^2 + 0.865s + 17.85\right).$$

The final open-loop shape is given in Fig. 4.

The prefilter, F, was set equal to the reference model, that is, $F = F_m$ so that the model matching specification becomes the plant-output disturbance rejection specification for which the standard loop shaping algorithm exists.

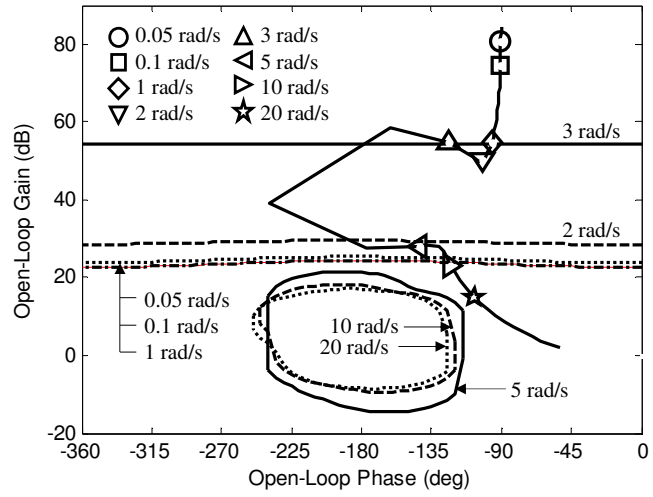

Fig. 4 Open-loop shaping: final shape.

C. Input Shaper, IS

The ZVD[k] input shaper [16] was selected in this paper due to its popularity and its closed-form formula. The formulas for its normalized impulse amplitudes, A_i, and time locations, t_i, are given by

$$A_i = \frac{\binom{k+1}{i-1}K^{i-1}}{\sum_{j=0}^{k+1}\binom{k+1}{j}K^j}, \quad t_i = (i-1)\frac{\pi}{\omega_n\sqrt{1-\zeta^2}},$$
$$i = 1, 2, ..., k+2,$$

where

$$K = e^{-\frac{\zeta\pi}{\sqrt{1-\zeta^2}}}.$$

$$\binom{n}{r} = \frac{n!}{r!(n-r)!}$$

is the combinations of n things taken r at a time.

The input shaper in the continuous time is then given by

$$IS(s) = \sum_{i=1}^{k+2} A_i e^{-t_i s}. \tag{4}$$

D. Simulation Result

Via simulation, several benefits of the proposed technique are highlighted in this section.

1) Require Shorter Input Shaper Length

Fig. 5(Top) shows the Bode magnitude plots of the model, F_m, and the inner-loop system, $PGF/(1+PG)$, for all 27 uncertain plants. The inner-loop system matches the model well, according to the model matching specification (3). Without the inner-loop system, Fig. 5(Bottom) shows large variation of the Bode magnitude plots of the 27 uncertain plants.

Percentage vibration, V, is a popular measure of vibratory level [16]. Its formula is given by

$$V = e^{-\zeta\omega_n t_n(\omega/\omega_n)}\left|\sum_{i=1}^{n} A_i e^{-t_i s_p(\omega/\omega_n)}\right|,$$

where ω is the actual natural frequency, ω_n is the model natural frequency, $s_p = -\zeta\omega_n - j\omega_n\sqrt{1-\zeta^2}$ is one of the system's flexible poles, ζ is the damping ratio, A_i and t_i, $i = 1, 2, ..., n$, are the amplitudes and time locations of the impulses.

Fig. 6 shows the input shaper length as a function of the percentage vibration, V. The input shaper length equals the time location of the last impulse, t_{k+2}. The dashed line shows the input shaper length required by the system without the inner-loop model matching. The solid line shows that of the system with the inner loop. With 50% uncertainty in c_1, c_2, and k_2, the input shaper length required by the system without the inner loop increases as the desired percentage vibration, V, decreases.

With the inner-loop model matching, the input shaper is designed from a fixed reference model, F_m; therefore, the input shaper length does not increase when less percentage vibration is required. From Fig. 6, when the desired percentage vibration is 43.53%, system either with or without the inner-loop system requires the input shaper length of 0.9802 s, which is the length of the ZV input shaper. However, when 3.59% percentage vibration is needed, the system without the inner loop requires 3.92 s of input shaper length, which is 4 times of that with the inner loop. Long input shaper length means longer time delay in the feedback loop, which limits the controller performance.

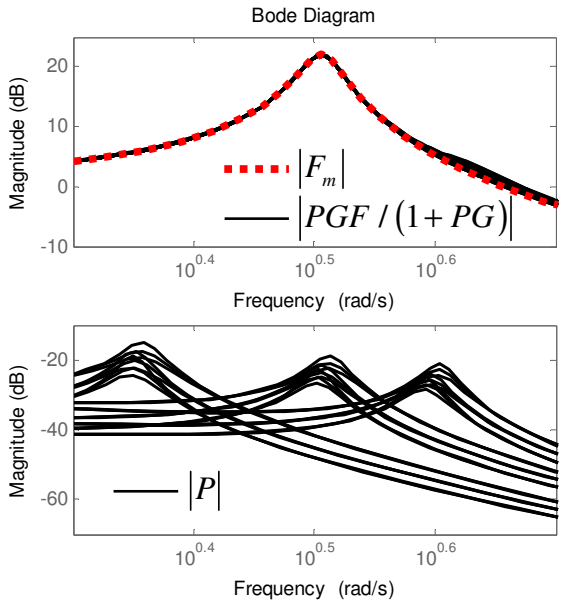

Fig. 5 Bode magnitude plots. (Top) With model matching. (Bottom) Without model matching.

For a fixed percentage vibration, $V = 10\%$, Fig. 7 shows plots between the uncertainty percentage in c_1, c_2, and k_2 and the input shaper length, with and without the inner loop. For larger uncertainty, longer input shaper length is required without the inner loop.

2) Increase Controller Bandwidth

From Fig. 7, for a fixed percentage vibration of $V = 10\%$ and an uncertainty of 50%, the ZVD^2 input shaper is required without the inner loop whereas only the ZV input shaper is required when the inner loop is present. From (4), the time delay of the ZVD^2 input shaper is triple that of the ZV input shaper. This increasing time delay limits the performance of the feedback controller, C.

To illustrate this, the controller, C, was chosen as the proportional-integral (PI) controller. From automated tuning of the PI controller, the controller is

$$C(s) = 1.742(1 + 0.19s)/s, \quad (5)$$

with the inner-loop model matching and the ZV input shaper, and

$$C(s) = 0.396(1 + 24s)/s,$$

without the inner loop and with the ZVD^2 input shaper. Fig. 8(Top) shows the Bode magnitude plots of the closed-loop system with the inner loop for all 27 plant variations and Fig. 8(Bottom) shows those without the inner loop. The closed-loop bandwidth is reduced from 3.4 rad/s with the inner loop to 0.1 rad/s without the inner loop. This clearly shows that the proposed system uses shorter time delay; therefore, the controller bandwidth can be increased.

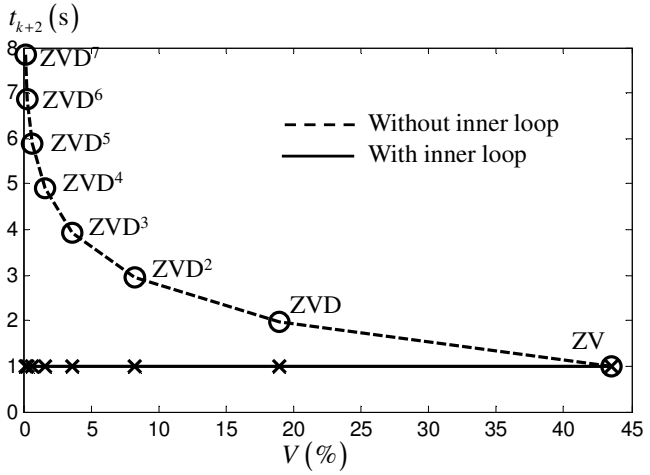

Fig. 6 Input shaper length as a function of percentage vibration: with and without inner loop.

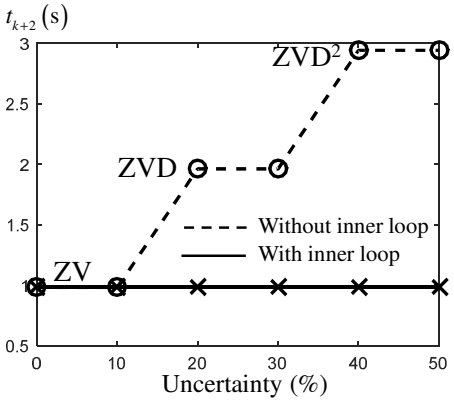

Fig. 7 Input shaper length as a function of uncertainty percentage: with and without inner loop.

Another problem concerns the instability of the closed-loop system without the inner-loop model matching. Fig. 9 shows its root locus plots. Without the inner-loop model matching, the plant, P, is quite uncertain, and the uncertain poles may unintentionally cross to the unstable right-half plane.

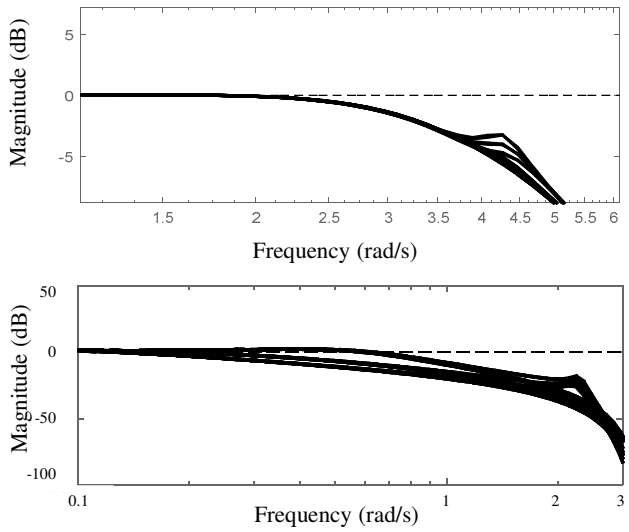

Fig. 8 Bode magnitude plots of the closed-loop systems. (Top) With the inner loop. (Bottom) Without the inner loop.

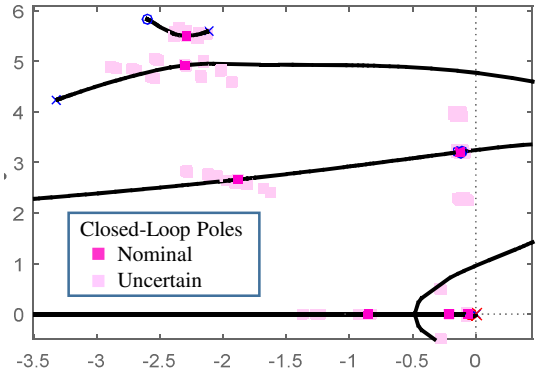

Fig. 9 Root locus plot without the inner-loop model matching.

3) Apply to Time-Varying Plant

Time-varying plant has the same effect as uncertain plant in that the actual plant will differ from the plant model used in designing the controller.

With the inner-loop model matching, the inner-loop system is designed to match a reference model well for all plant variations as specified by the uncertainty percentage. As a result, the tracking as well as the vibration suppression performances will not be deteriorate when the plant is time-varying.

Fig. 10 shows the tracking results of the flexible output, y. The solid lines are the flexible output; the dotted lines are the reference, r_b. Fig. 10(a)-(c) are for the system without the inner-loop model matching. Fig. 10(d) is for the system with the inner loop. The plant parameters, c_1, c_2, and k_2, were deviated from their nominal values according to a formula

$$\text{Actual value} = \text{Nominal value} * (1 - \%\,\text{uncertainty}/100).$$

Fig. 10(a)-(c) clearly show the deteriorated vibration suppression performance without the inner loop when the uncertainty percentage increases. With the inner loop, the vibration suppression performance does not degrade significantly even with uncertainty as high as 70%.

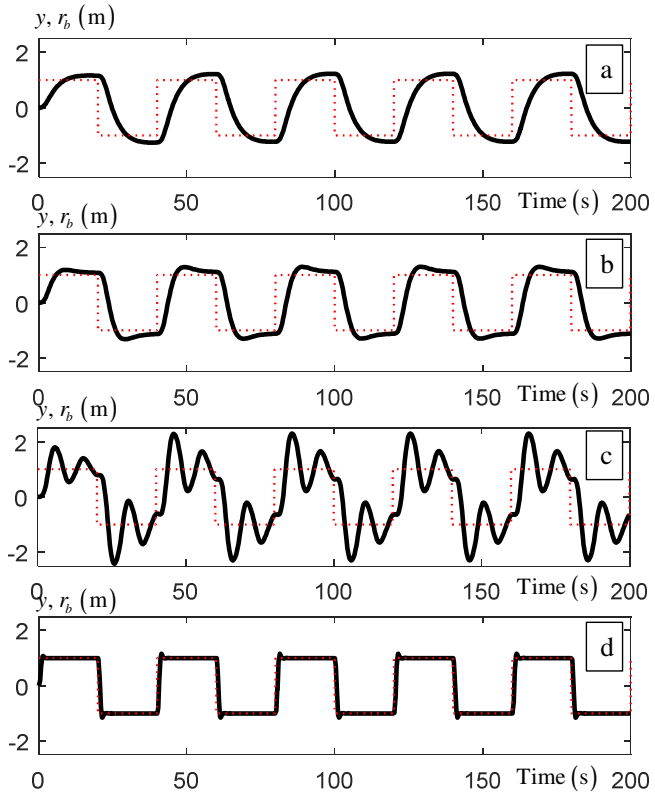

Fig. 10 Flexible output, y, and its baseline reference. Without inner loop: (a) 0% uncertainty, (b) 35% uncertainty, (c) 70% uncertainty. With inner loop: (d) 70% uncertainty.

4) Reduce Cost of Feedback

Can the reference model, F_m, be made critically or overly damped instead of underdamped, hence there is no need for the input shaper, *IS*?

Since the input shaper is a feed-forward filter, it merely changes the input signal to avoid exciting the flexible modes. Therefore, one benefit of using the input shaper with underdamped reference model is to reduce cost of feedback.

Also, in general, underdamped system $(0 < \zeta < 1)$ has quicker transient response than that of the critically damped $(\zeta = 1)$ and overly damped $(\zeta > 1)$ systems.

To illustrate this, a critically damped version of the reference model (1), which is

$$F_m(s) = \frac{(3.2074)^2}{s^2 + 2(1)(3.2074)s + (3.2074)^2},$$

was used in the simulation, without the input shaper, *IS*. A new controller, *G*, was re-designed using the quantitative feedback theory as

$$G = 24.75(s + 0.68)(s^2 + 4.89s + 16).$$

The pre-filter was given by $F = F_m$, and the feedback controller remained the same as (5).

Fig. 11(a) shows the flexible output, *y*, and its reference, r_b. Fig. 11(b) contains the control effort, *u*. Fig. 11(c) and (d) are those for the proposed underdamped reference model with the input shaper. Quicker transient response can be seen using the proposed system by comparing Fig. 11(a) to (c). The control effort is also reduced by the proposed system by comparing Fig. 11(b) to (d).

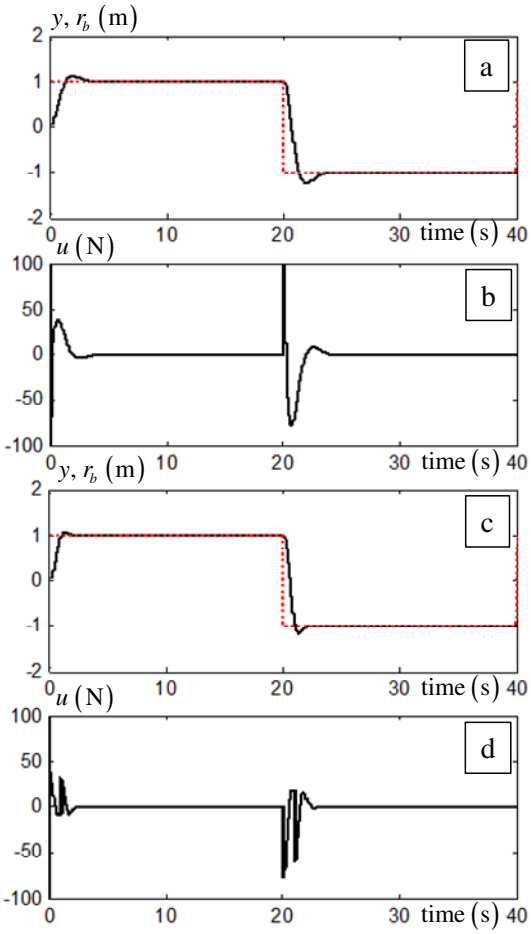

Fig. 11 Critically damped case: (a) flexible output and its reference and (b) control effort. Underdamped case: (c) flexible output and its reference and (d) control effort.

EXPERIMENT

To show the applicability of the proposed inner-loop model matching system, the technique was applied to a flexible-joint robot in Fig. 12.

Two optical encoders measure the motor shaft and the link angular positions. A National Instruments· Labview system was used as the computer controlled system.

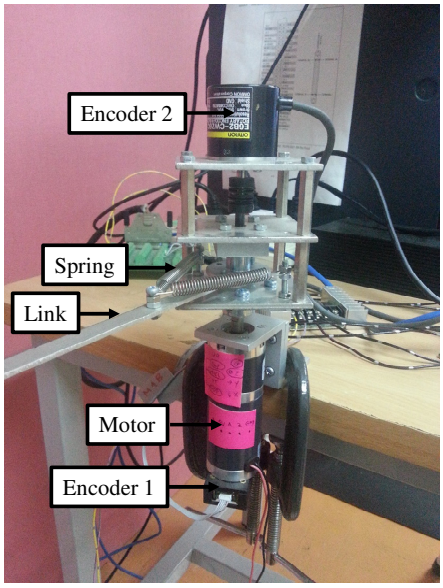

Fig. 12 Flexible-joint robot in the experiment.

A. Plant, P

The equations of motion of the flexible-joint robot are analogous to those of the two-mass system in Fig. 2. System identification of the robot consists of two steps. First, the motor hub was rotated manually while the motor shaft position, x_1, and the link position, x_2, were measured. The Matlab GUI, *ident*, was used to identify a transfer function from x_1 to x_2 as

$$P_2(s) = \frac{X_2}{X_1} = \frac{41.09s + 3173}{s^2 + 16.42s + 3161}.$$

Fig. 13(a) shows the modeled link position (in solid line) versus the actual link position (in dashed line). Second, a frequency-varying sine wave was given as a reference for the motor shaft position to follow using a proportional controller. Both motor shaft position, x_1, and the control effort, *u*, given to the motor driver board, were recorded. A transfer function from *u* to x_1 was found as

$$P_1(s) = \frac{X_1}{U} = \frac{140.5s^2 + 1.107\times10^4 s + 1403}{s^4 + 15.1s^3 + 852.8s^2 + 1068s}.$$

Fig. 13(b) shows the modeled motor shaft position (in solid line) versus the actual shaft position (in dashed line). Several experiments were repeated to validate the models.

The overall plant, $P(s) = P_1(s)P_2(s)$, has two flexible modes whose parameters are $\omega_{n1} = 28.90$ rad/s, $\zeta_1 = 0.239$, and $\omega_{n2} = 56.22$ rad/s, $\zeta_2 = 0.146$.

B. Closed-Loop System

The closed-loop system, used in the robotic experiment, is shown in Fig. 14. Note that the motor shaft position, x_1, was used as feedback for model matching rather than the link position, x_2, because of the stability issue.

The reference model was chosen as

$$F_m(s) = \frac{(5)^2}{s^2 + 2(0.7)(5)s + (5)^2},$$

whose $\omega_n = 5$ rad/s and $\zeta = 0.7$. A different choice of $F_m(s)$ is also possible.

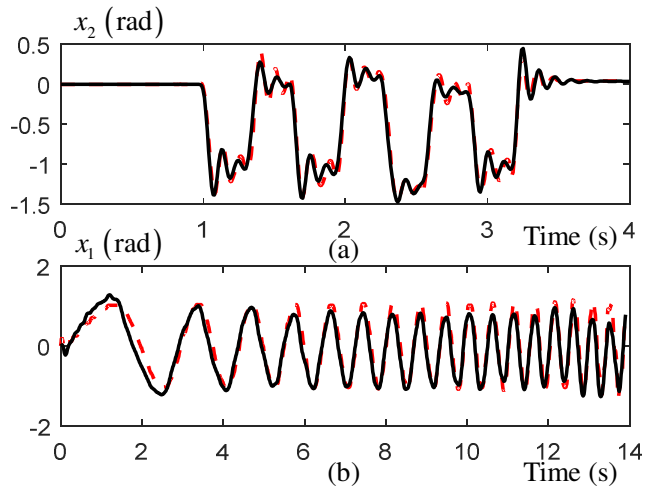

Fig. 13 System identification result. (a) Link position. (b) Motor shaft position.

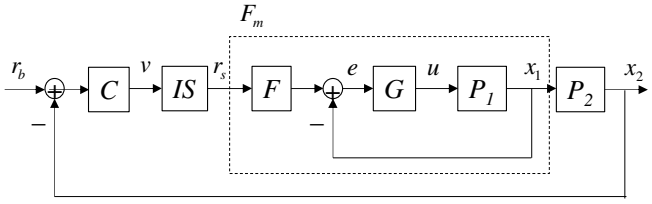

Fig. 14 Closed-loop signal shaping with inner-loop model matching.

The stability margin specification (2) and the model matching specification (3) were enforced. From the open-loop shape, it was sufficient to use a simple gain, $G(s) = 3$. The pre-filter was set equal to the reference model, that is, $F = F_m$.

Two ZVD input shaping filters (4) were cascaded. They were designed using the mode parameters, ω_{n2} and ζ_2, of $P_2(s)$ and, ω_n and ζ, of $F_m(s)$.

The controller, C, was chosen as a PI controller

$$C(s) = 0.015\left(1 + \frac{1}{0.01s}\right).$$

For comparison, the traditional closed-loop signal shaping system, whose diagram is shown in Fig. 15, was also implemented. The same controller, C, was used. However, the input shaper, IS, was designed using the mode parameters of the plant, P, which are ω_{n1}, ζ_1 and ω_{n2}, ζ_2.

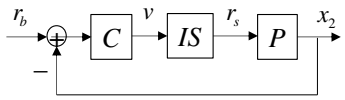

Fig. 15 Traditional closed-loop signal shaping.

C. Experimental Result

Fig. 16 shows the tracking result. The link angular position, x_2, is plotted in solid line versus its reference, r_b, in dotted line. Fig. 16(a) is of the proposed CLSS with inner-loop model matching whereas Fig. 16(b) is of the traditional CLSS. The link position oscillated more when the traditional CLSS was used. Even though there is the input shaper, designed to suppress the vibratory modes of the plant, the oscillation comes from the feedback controller, C. To see this clearly, Fig. 17 compares the control effort used by the proposed technique (Fig. 17(a)) to that used by the traditional CLSS (Fig. 17(b)). Because the proposed technique reduces the cost of feedback, as discussed earlier in the simulation section, its control effort has more distribution and lower peak.

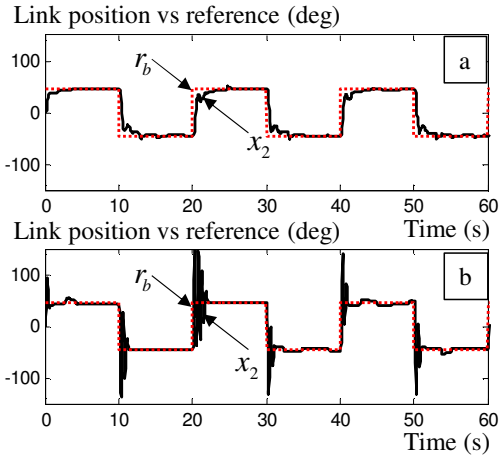

Fig. 16 Link position (in solid line) versus its reference (in dotted line). (a) Proposed CLSS with inner-loop model matching. (b) Traditional CLSS.

Fig. 18(a) shows the model matching performance by plotting the motor shaft position, x_1, versus the output, x_m, from the reference model, F_m. Because x_1 closely matches x_m, the inner-loop system matches the reference model, F_m. When the plant is uncertain, for example, the payload at the tip was increased by 30% in the experiment, similar tracking result to that of Fig. 16(a) was obtained.

Fig. 18(b) is a result of placing an angular velocity measurement sensor at the robot tip. The dotted line is of the traditional CLSS whereas the solid line is of the proposed CLSS

with inner-loop modeling matching. The traditional CLSS has approximately five times more vibration than the proposed CLSS.

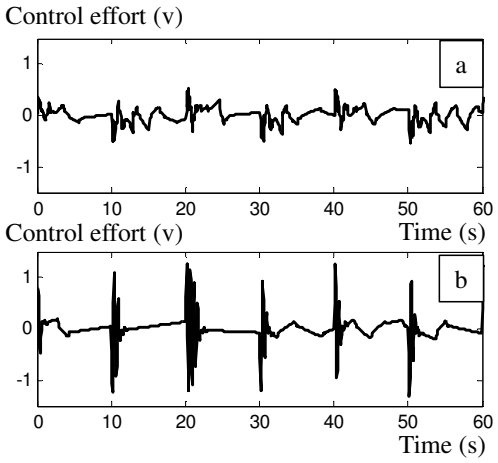

Fig. 17 (a) Control effort of the proposed technique. (b) Control effort of traditional CLSS.

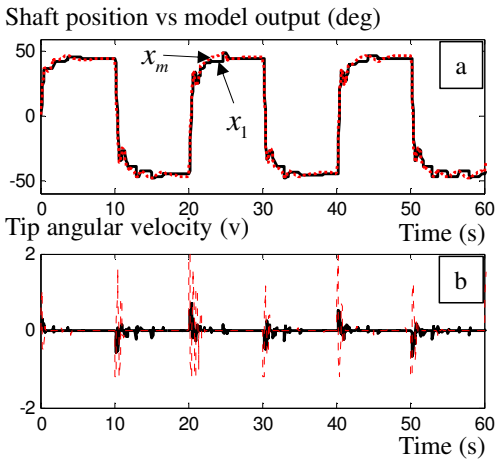

Fig. 18 (a) Motor shaft position (in solid line) versus reference model output (in dotted line) of the proposed technique. (b) Tip angular velocity of the proposed technique (in solid line) versus that of traditional CLSS (in dotted line).

CONCLUSIONS

A novel technique is proposed in this paper. An inner-loop feedback controller is used to match the uncertain flexible plant to an exact reference model. As a result, the closed-loop input shaper can be designed from the exact model and can be shorten. This leads to reduction in the time delay in the feedback loop and increasing of control bandwidth. The technique also applies to time-varying or nonlinear plants.

Future work includes applying this technique to manual control of flexible systems in which a human operator is the outer-loop feedback controller. A more rigorous proof on the reduction of cost of feedback is also the future work.

ACKNOWLEDGMENT

The authors would like to thank Craig Borghesani and Terasoft for their evaluation copy of the QFT Toolbox.

REFERENCES

[1] O. J. M. Smith, "Posicast control of damped oscillatory systems," *Proceedings of the IRE*, vol. 45, no. 9, pp. 1249–1255, Sep. 1957.

[2] J. R. Huey and W. Singhose, "Trends in the stability properties of CLSS controllers: a root-locus analysis," *IEEE Transactions on Control Systems Technology*, vol. 18, no. 5, pp. 1044–1056, Sep. 2010.

[3] R. Tang and J. Huang, "Control of bridge cranes with distributed-mass payloads under windy conditions," *Mechanical Systems and Signal Processing*, vol. 72–73, pp. 409–419, May 2016.

[4] M. J. Maghsoudi, Z. Mohamed, A. R. Husain, and M. O. Tokhi, "An optimal performance control scheme for a 3D crane," Mechanical Systems and Signal Processing, vol. 66–67, pp. 756–768, Jan. 2016.

[5] J. J. Potter, C. J. Adams, and W. Singhose, "A planar experimental remote-controlled helicopter with a suspended load," *IEEE/ASME Transactions on Mechatronics*, vol. 20, no. 5, pp. 2496–2503, Oct. 2015.

[6] W. Chatlatanagulchai, P. Poedaeng, and N. Pongpanich, "Improving closed-loop signal shaping of flexible systems with Smith predictor and quantitative feedback," *Engineering Journal*, vol. 20, pp. 1–13, Oct. 2016.

[7] M.-C. Pai, "Robust input shaping control for multi-mode flexible structures using neuro-sliding mode output feedback control," *J. of the Franklin Institute*, vol. 349, no. 3, pp. 1283–1303, Apr. 2012.

[8] Z. N. Masoud and K. A. Alhazza, "Frequency-modulation input shaping control of double pendulum overhead cranes," *J. of Dynamic Systems, Measurement, and Control*, vol. 136, no. 2, pp. 1–11, Mar. 2014.

[9] D. Yuan and T. Chang, "Model reference input shaper design with applications to a high-speed robotic workcell with variable loads," *IEEE Trans. on Industrial Electronics*, vol. 55, no. 2, pp. 842–851, Feb. 2008.

[10] J. Han, Z. Zhu, Y. He, and J. Qi, "A novel input shaping method based on system output," *J. of Sound and Vibration*, vol. 335, pp. 338–349, Jan. 2015.

[11] L. Yu and T. N. Chang, "Model reference zero vibration control of ultrahigh precision piezoelectric nanopositioner," in *Proc. ACC 2010*, Baltimore, MD, pp. 5856–5861.

[12] D. Fujioka and W. Singhose, "Control effort reduction analysis of zero-vibration model reference control for controlling a time-varying plant," in *Proc. ACC 2014*, Portland, OR, pp. 3110–3115.

[13] W. Chatlatanagulchai and P. Kaveesoontornsanoh, "Improving robustness of input shaping technique with model reference iterative learning control," in *Proc. MENETT 2014*, Khonkaen, Thailand, pp. 1–6.

[14] W. Chatlatanagulchai, D. Kijdech, T. Benjalersyarnon, and S. Damyot, "Quantitative feedback input shaping for flexible-joint robot manipulator," *J. of Dynamic Systems, Measurement and Control*, vol. 138, no. 6, pp. 1–10, Jun. 2016.

[15] I. Horowitz, *Quantitative Feedback Design Theory*. Boulder, CO: QFT Publications, 1993, pp. 1–486.

[16] N. C. Singer and W. C. Seering, "Preshaping command inputs to reduce system vibration," *J. of Dynamic Systems, Measurement and Control*, vol. 112, no. 1, pp. 76–82, Mar. 1990.